Eur. J. Biochem. *171*, 479–484 (1988)

Determination of the backbone conformation of secretin by restrained molecular dynamics on the basis of interproton distance data

G. Marius CLORE[1], Michael NILGES[1], Axel BRÜNGER[2] and Angela M. GRONENBORN[1]

[1] Max-Planck-Institut für Biochemie, Martinsried bei München
[2] Department of Molecular Biophysics and Biochemistry and the Howard Hughes Medical Institute, Yale University, New Haven, Connecticut

(Received August 13/October 19, 1987) – EJB 87 0961

The backbone conformation of the 27-residue polypeptide hormone secretin has been investigated using nuclear magnetic resonance spectroscopy and restrained molecular dynamics calculations under conditions where it adopts a fully ordered structure (40% v/v trifluoroethanol). The basis for the restrained molecular dynamics calculations consists of 52 nuclear-Overhauser-enhancement-derived interproton distance restraints involving the NH, $C^{\alpha}H$ and $C^{\beta}H$ protons. It is shown that convergence to similar extended structures is achieved starting from four different initial structures, namely an α helix, a mixed α/β structure, a β strand and a polyproline helix. The converged structures are made up of short N- and C-terminal strand-like regions and a central region comprising two irregular helices connected by a 'half-turn'.

It has long been presumed that small peptide hormones which have random coil conformations in free solution, adopt an ordered conformation on binding to their membrane-bound receptor [1]. Recent studies using both CD and NMR spectroscopy have shown that in the case of three such hormones, glucagon, the 1–29 fragment of growth-hormone-releasing factor and secretin, ordered structures are formed under conditions of reduced water activity, such as the presence of moderate amounts (30–40% v/v) of trifluoroethanol or detergent micelles [2–5]. Based on a qualitative interpretation of nuclear Overhauser enhancement (NOE) data, the conformations adopted by these three peptide hormones under such conditions appear to be similar, comprising a short N-terminal strand-like region followed by two helices connected by a 'half-turn' [3–5]. Further, as no NOEs between residues more than five apart in the sequence could be detected, it was deduced that they probably form extended non-globular structures. In the case of glucagon these deductions have been partially confirmed by means of distance geometry calculations carried out on the basis of NOE-derived interproton distance restraints [3]. As these calculations, however, were carried out on three separate partially overlapping fragments of glucagon rather than on the complete molecule, a global view of the structure could not be obtained.

It has recently been shown that the structures of globular proteins can be reliably determined from interproton distances less than 0.5 nm by means of both distance geometry [6, 7] and restrained molecular dynamics [8] calculations. The structure determination of globular proteins, however, is aided by the fact that the distance set consists not only of short-range distances (i.e. $|i-j| \leq 5$ where i and j are residue numbers) but also long-range ($|i-j| > 5$) ones. These long-range distances are crucial in restricting the size of the conformational space consistent with the experimental data, thereby simplifying the task of locating the global minimum energy region. In contrast to globular structures, such long-range distances are absent in extended molecules so that the structure determination is rendered considerably more difficult.

In this paper we extend our previous NMR study on secretin [5] to the determination of its backbone conformation(s) by means of restrained molecular dynamics calculations [8–12] based on NOE-derived interproton distance restraints. We show that the short range NOE data are indeed sufficient to define the overall structure within certain well-defined limits and that convergence to similar structures is achieved starting from four different initial structures, namely an α helix, a mixed α/β structure, an extended β strand and a polyproline helix.

METHODS

Secretin was a gift from Dr W. Koenig (Hoechst AG, FRG) and was > 99% pure as judged by HPLC. Samples for NMR contained 5.6 mM secretin in 30 mM sodium phosphate buffer pH 6.5, 40% (v/v) (D_3)trifluoroethanol and either 60% D_2O or 54% H_2O/6% D_2O. All NMR spectra were recorded at 20°C on a Bruker AM500 spectrometer. NOESY spectra [13] were recorded in the pure phase absorption mode [14] using the conditions reported previously [5].

All energy minimization and restrained molecular dynamics calculations were carried out as described previously [8] on a CRAY-XMP using the program XPLOR (ATB, unpublished data) which is a version of the program CHARMM [15] especially adapted for restrained molecular dynamics calculations. Note that the conformation about the peptide bond is assumed to be planar and *trans*.

Correspondence to G. M. Clore, Max-Planck Institut für Biochemie, D-8033 Martinsried bei München, Federal Republic of Germany

Abbreviations. NOESY, two-dimensional NOE spectroscopy; rms, root mean square.

RESULTS AND DISCUSSION

Interproton distance restraints and calculational strategy

As no NOEs involving side chains (excluding $C^{\beta}H$ protons) were observed in the NOESY spectra, presumably due to their high mobility, only NOEs involving NH, $C^{\alpha}H$ and $C^{\beta}H$ protons were available to derive a set of approximate interproton distance restraints. Thus, the NOEs used comprise all those summarized in Fig. 5 of [5] with the exception of the $C^{\beta}H(i) - NH(i+1)$ NOEs which carry no structural information in the absence of other interresidue NOEs involving side-chain protons. The resulting data set comprised a total of 52 NOEs of which 44 involved only NH and $C^{\alpha}H$ protons and the remaining 8 consisted of $C^{\alpha}H(i) - C^{\beta}H(j)$ NOEs. The NOEs were classified into strong, medium and weak from the 100-ms NOESY spectra and then converted into distance ranges of 0.18 – 0.27 nm, 0.18 – 0.33 nm and 0.18 – 0.50 nm, respectively. These distance restraints were included in the total energy function of the system in the form of square-well effective potentials [11].

The restrained molecular dynamics calculations were carried out starting from four different initial structures: an α helix (ϕ, ψ = $-57°$, $-47°$) known as IniI; a mixed α/β structure known as IniII in which residues 1–7, 13–17 and 25–27 were in the form of an extended β strand and residues 7–13 and 17–25 were in the form of an α helix; an extended β strand (ϕ, ψ = $-139°$, $135°$) known as IniIII; and a polyproline helix (ϕ, ψ = $-80°$, $150°$) known as IniIV. The range of α-helices in IniII was based on their approximate location deduced from a qualitative interpretation of the NOE data [5]. The four initial structures are shown in Fig. 1.

The protocol of restrained dynamics used is summarized in Table 1 and was designed to overcome large energy barriers and to achieve convergence in as short a computer time as possible. Three calculations were carried out for each initial structure using different random number seeds for the assignment of initial velocities. Thus IniI gives rise to three restrained dynamics structures known collectively as ⟨RDI⟩, and similarly for the other initial structures. Although the calculations were carried out with side chains, only the backbone conformations are analysed as the side-chain conformations are not defined by the NOE restraints.

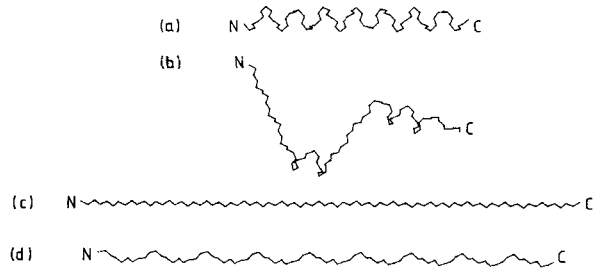

Fig. 1. *The four initial structures.* (a) IniI is an α helix, (b) IniII a mixed α/β structure, (c) IniIII an extended β strand and (d) IniIV a polyproline helix

Table 1. *Protocol of the restrained dynamics structure determination*
c is the NOE restraints force constant; in phase 2 this was increased as indicated by doubling its value every 0.0375 ps. In phases 1 and 2 the $C^{\alpha}H(i) - C^{\beta}H(j)$ distance restraints were applied as $\langle r_c \rangle$ centre averages with 0.1 nm added to their upper limits; in phases 3 and 4 they were applied as $\langle r^{-6} \rangle$ averages with no corrections to their upper limits. The temperature of the system was adjusted to lie between 1000 K and 8000 K in phase 2 by scaling the velocities of the atoms upwards by 1.5 if the temperature fell below 1000 K and downwards by a factor of 0.75 if the temperature increased above 8000 K. It should be noted that the temperature in these calculations has no physical meaning *per se* but simply reflects the velocities of the atoms

Phase 1	100 cycles restrained energy minimization c = 42 kJ · mol^{-1} · nm^{-2}
Phase 2	0.5625 ps restrained dynamics T = 1000–8000 K integration time step = 0.15 fs c = 42–42000 kJ · mol^{-1} · nm^{-2}
Phase 3	2 ps restrained dynamics cooling T cooled to 300 K integration time step = 0.5 fs c = 42000 kJ · mol^{-1} · nm^{-2}
Phase 4	100 cycles of restrained energy minimization c = 16720 kJ · mol^{-1} · nm^{-2}

The converged structures

The results of the restrained molecular dynamics calculations are summarized in Tables 2 and 3 and Figs 2 and 3. It is clear from this data that convergence to similar extended structures which satisfy the interproton distance restraints within their experimental errors (Table 3) is achieved starting from all four different initial structures. Further, the extended nature of the structures does not simply arise from the fact that IniI, IniIII and IniIV are extended, as IniII is distinctly kinked at its four α/β junctions (Fig. 1). In contrast, in the absence of experimental restraints, no convergence occurs either globally or locally.

Analysis of the atomic rms differences (Table 2 and Fig. 3) clearly shows that the converged structures can be divided into three regions: residues 1–6, 6–25 and 25–27. Within each region the structure is reasonably well-defined both globally and locally. However, the exact orientation of the three regions relative to each other cannot be defined. This is the principal source of the differences in the atomic rms differences between structures starting from the same initial structure and from different initial structures (cf. Figs 2 and 3 and Table 2). Thus, within each region, the atomic rms differences are comparable in both cases. For the whole molecule, however, the differences are much smaller for the former case than the latter. Considering the energies of the structures (only backbone atoms), it is apparent that the higher the restraint energies of the initial structure, the higher both the restraint energy and the non-bonding energy of the converged structures (Table 3). Not surprisingly, this is also correlated with the magnitude of the atomic rms differences between the initial structures and the final converged structures ($\approx 1.3-1.5$ nm for IniIII and IniIV compared to $\approx 0.3-0.5$ nm for IniI and IniII; Table 2). Nevertheless, although the NOE restraint energy of the ⟨RDIII⟩ and ⟨RDIV⟩ structures is a factor of about three larger than those of the ⟨RDI⟩ and ⟨RDII⟩ structures (Table 4), the interproton distance deviations between calculated and experimental distances for ⟨RDIII⟩ and ⟨RDIV⟩ are still within the experimental errors and no deviations larger than 0.05 nm are observed (Table 3). It should also be noted that the largest differences with respect to interproton distance deviations between ⟨RDI⟩ and ⟨RDII⟩

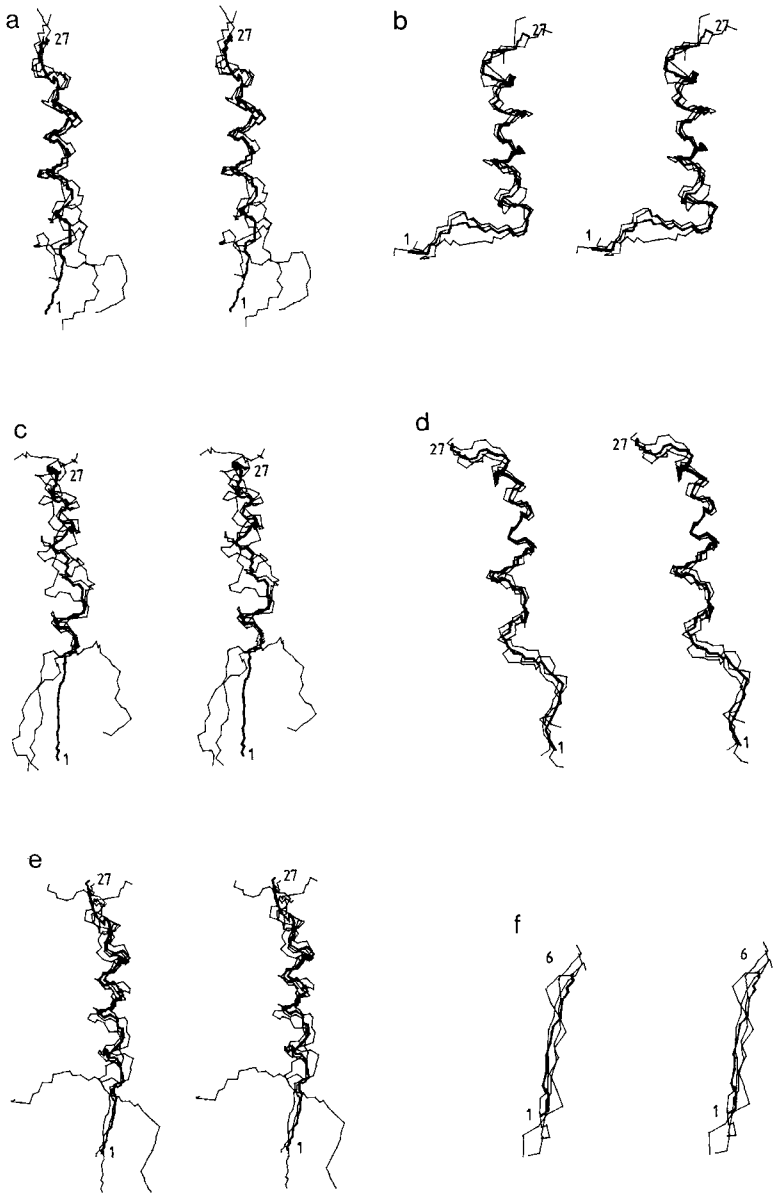

Fig. 2. *Best-fit superpositions of the converged structures.* (a) ⟨RDI⟩ vs $\overline{\text{RDI}}$; (b) ⟨RDII⟩ vs $\overline{\text{RDII}}$; (c) ⟨RDIII⟩ vs $\overline{\text{RDIII}}$; (d) ⟨RDIV⟩ vs $\overline{\text{RDIV}}$; (e) and (f) ⟨RD⟩ vs $\overline{\text{RD}}$. The views in a–f are best fitted to residues 6–15 and 17–25 while that in (f) is best fitted to residues 1–6. The notation of the structures is the same as that in Table 2; in addition, ⟨RD⟩ denotes collectively the mean structures $\overline{\text{RDI}}$, $\overline{\text{RDII}}$, $\overline{\text{RDIII}}$ and $\overline{\text{RDIV}}$. The mean structures in a–d are shown as thick lines whereas the individual restrained dynamics structures are shown as thin lines. In e and f the overall mean structure $\overline{\text{RD}}$ is shown as a thick line, and the individual mean structures ⟨RD⟩ derived from the four different sets of restrained dynamics structures are shown as thin lines

on the one hand, and ⟨RDIII⟩ and ⟨RDIV⟩ on the other, involve the $C^{\alpha}H(i) - C^{\beta}H(j)$ distances (Table 3).

In considering the results of these calculations, one should bear in mind the question of the possible existence of more than one significantly different conformation and the effect that this could have on the results. As only a single resonance is observed per proton in the NMR spectrum [5], one can deduce that either there is only one conformation present or, alternatively, there are multiple conformations in fast exchange on the chemical shift scale. The circular dichroic measurements [5] demonstrated that a conformational transition is complete at a concentration of 40% (v/v) trifluoroethanol. While this may mean that the formation of the helical regions is complete, it clearly need not imply that all of the peptide is in a single conformation. The same is true of the NOE measurements. While they may appear to be consistent with a single conformation, they do not exclude the possibility of multiple conformations. Fortunately, difficulties that may arise from such a situation can be dealt with based on the fact that the magnitude of the NOE at short mixing times, under conditions of fast exchange, is proportional to $\Sigma a_i r_i^{-6}$ where a_i is the proportion of species i present and r_i is the value of a particular interproton distance in species i. Consequently, all the distance limits derived from the NOE data will be heavily weighted towards the particular conformation for which a given distance is shortest, providing this conformation

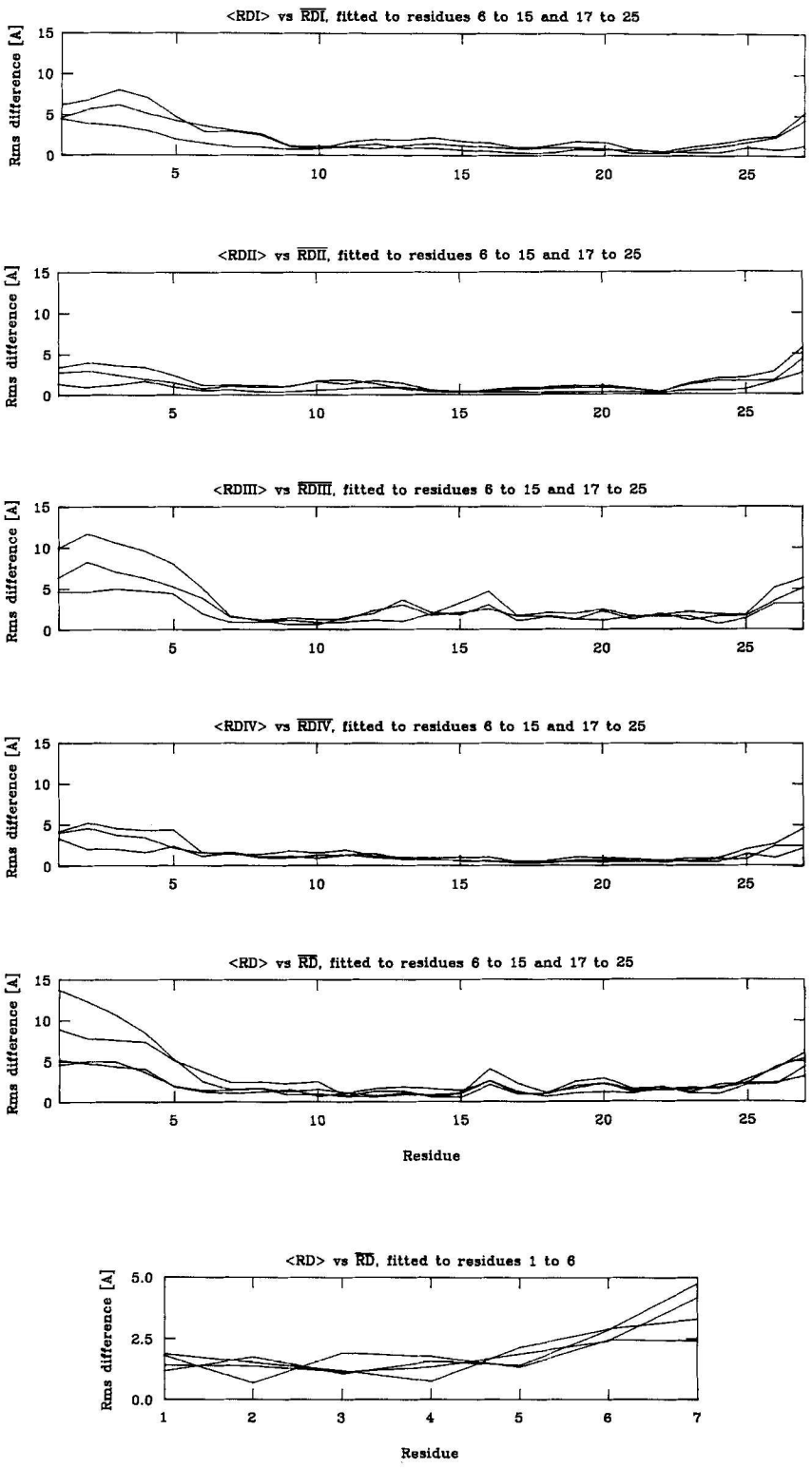

Fig. 3. *Atomic rms distributions of the backbone (N, C^{α}, C and O) atoms of the individual structures about their respective mean structures.* The notation of the structures is the same as that in Table 2 and Fig. 2, and the six successive plots correspond to the stereoviews a–f shown in Fig. 2. rms differences are plotted in Å (1 Å ≡ 0.1 nm)

constitutes a major species. Under these circumstances, it is unlikely that several major species exhibiting significantly different conformations (e.g. extended strand versus helix) could satisfy all the restraints at the same time. Minor species (constituting about 10% or less), on the other hand, are unlikely to contribute significantly to the measured NOEs as the observed cross-relaxation rate for a given proton pair is simply the weighted average of the cross-relaxation rates of the con-

Table 2. *Backbone atomic rms differences*
The notation of the structures is as follows. IniI, IniII, IniIII and IniIV are the initial structures. IniI is a regular α helix; IniII a mixed α-helix/β-strand structure (with residues 1–6, 15–17 and 25–27 in the form of β strands, residues 7–15 and 17–25 in the form of α helices), IniIII a regular β strand, and IniIV a regular polyproline helix. ⟨RDI⟩, ⟨RDII⟩, ⟨RDIII⟩ and ⟨RDIV⟩ are the restrained dynamics structures derived from each initial structure, and for each initial structure there are three restrained dynamics structures obtained by using different random number seeds for the assignment of the initial velocities. $\overline{\text{RDI}}$, $\overline{\text{RDII}}$, $\overline{\text{RDIII}}$ and $\overline{\text{RDIV}}$ are the mean structures obtained by averaging the coordinates of the ⟨RDI⟩, ⟨RDII⟩, ⟨RDIII⟩ and ⟨RDIV⟩ structures, respectively, best fitted to all residues. $\overline{\text{RD}}$ is the mean structure obtained by averaging the coordinates of all twelve restrained dynamics structures best fitted to residues 6–15 and 17–25

	Difference structures	Backbone (N, C^{α}, C, O) atomic rms difference for		
		all residues	residues 6–15 and 17–25	residues 1–6
		nm		
Atomic rms differences between initial structures	IniI vs IniII	0.56	0.31	0.38
	IniI vs IniIII	1.51	1.11	0.38
	IniI vs IniIV	1.28	0.94	0.34
	IniII vs IniIII	1.62	1.04	0
	IniII vs IniIV	1.40	0.89	0.15
	IniIII vs IniIV	0.27	0.22	0.15
Atomic rms shifts	$\overline{\text{RD}}$ vs IniI	0.27	0.22	0.21
	$\overline{\text{RD}}$ vs IniII	0.50	0.29	0.28
	$\overline{\text{RD}}$ vs IniIII	1.57	1.15	0.28
	$\overline{\text{RD}}$ vs IniIV	1.34	0.99	0.24
Atomic rms distributions	$\overline{\text{RD}}$ vs ⟨RDI⟩	0.28 ± 0.05	1.9 ± 0.04	0.22 ± 0.04
	$\overline{\text{RD}}$ vs ⟨RDII⟩	0.36 ± 0.01	1.8 ± 0.02	0.22 ± 0.02
	$\overline{\text{RD}}$ vs ⟨RDIII⟩	0.33 ± 0.04	2.2 ± 0.04	0.23 ± 0.02
	$\overline{\text{RD}}$ vs ⟨RDIV⟩	0.33 ± 0.03	2.1 ± 0.02	0.22 ± 0.01
	$\overline{\text{RD}}$ vs $\overline{\text{RDI}}$	0.21	0.15	0.18
	$\overline{\text{RD}}$ vs $\overline{\text{RDII}}$	0.34	0.15	0.18
	$\overline{\text{RD}}$ vs $\overline{\text{RDIII}}$	0.20	0.13	0.19
	$\overline{\text{RD}}$ vs $\overline{\text{RDIV}}$	0.29	0.18	0.17
	⟨RDI⟩ vs $\overline{\text{RDI}}$	0.19 ± 0.06	0.13 ± 0.04	0.10 ± 0.02
	⟨RDII⟩ vs $\overline{\text{RDII}}$	0.13 ± 0.04	0.10 ± 0.04	0.12 ± 0.05
	⟨RDIII⟩ vs $\overline{\text{RDIII}}$	0.26 ± 0.05	0.17 ± 0.01	0.15 ± 0.03
	⟨RDIV⟩ vs $\overline{\text{RDIV}}$	0.16 ± 0.01	0.10 ± 0.01	0.14 ± 0.03
	$\overline{\text{RDI}}$ vs $\overline{\text{RDII}}$	0.46	0.17	0.28
	$\overline{\text{RDI}}$ vs $\overline{\text{RDIII}}$	0.34	0.25	0.22
	$\overline{\text{RDI}}$ vs $\overline{\text{RDIV}}$	0.38	0.30	0.20
	$\overline{\text{RDII}}$ vs $\overline{\text{RDIII}}$	0.44	0.23	0.14
	$\overline{\text{RDII}}$ vs $\overline{\text{RDIV}}$	0.58	0.31	0.15
	$\overline{\text{RDIII}}$ vs $\overline{\text{RDIV}}$	0.27	0.22	0.14

tributing individual species, and as such will not be detectable. In the case of each restrained dynamics structure, all the restraints are indeed satisfied within their experimental errors (Table 3). Thus the difference between the restrained dynamics structures can be considered to provide a measure of the conformational space accessible to the peptide within the constraints imposed by the available interproton distance data. We therefore conclude that no assumption of the existence of a single conformation is required in this particular case. Rather, the results should be interpreted in terms of a ensemble of structures all of which satisfy the experimental interproton distance restraints.

The structural features that emerge are as follows. Residues 1–6 and 25–27 form short N- and C-terminal strand-like regions. The region from residues 1–6 is reasonably well defined locally (see Figs 2f and 3) but its orientation with respect to the rest of the molecule cannot be accurately ascertained. This is probably due to the absence of any NOEs bridging the Gly4-Thr5 junction. Nevertheless, it must be stressed that these terminal segments do not fold back on the rest of the molecule so that in all cases the overall structure is an extended one. The central region 6–25 is relatively well defined and is composed of two irregular helices (7–13 and 17–25) connected by what can be termed a 'half-turn', as predicted from a qualitative interpretation of the NOE data [5]. Within this central region, the conformation of residue 16 is less well defined compared to the other residues. Although the atomic positions are relatively well defined within each region, there is still some variability in the ϕ and ψ angles for each residue, with an average angular rms difference between all pairs of 60 ± 22° and 72 ± 23°, respectively. These values are comparable to those observed in analogous structure determinations of globular proteins [11, 12, 16].

An examination of the distribution of residue types is also of interest. We note that there are two hydrophobic patches which could constitute the main site of interaction with the

Table 3. *Interproton distance deviations, deviations from ideality, NOE energies and non-bonding energies*
The rms interproton distance deviations are calculated with respect to the upper and lower limits of the distance restraints [11]. The notation of the structures is the same as that in Table 2. The number of terms for the NOE restraints energy and for the bonds angles and improper torsions are given in parentheses. (The latter are the restraints used to maintain planarity and correct chirality at chiral centres.) The non-bonding energies are computed only for the backbone (N, NH, C^{α}, $C^{\alpha}H$, C, O), C^{β} and $C^{\beta}H$ atoms. The NOE restraints potential is represented by a square well potential [11] with a restraints force constant of 16720 kJ · mol^{-1} · nm^{-2}

Structures	rms difference between target and calculated interproton distances			Deviations from ideality			Energies		
	all	NH(i) – NH(j) NH(i) – $C^{\alpha}H$(j)	$C^{\alpha}H(i) - C^{\beta}H(j)$	bonds	angles	impropers	E_{NOE}	$E_{non\text{-}bonding}$	
	(52)	(44)	(8)	(230)	(380)	(77)	(52)		
	nm				degrees		kJ · mol^{-1} (kcal · mol^{-1})		
Initial									
IniI	0.060	0.064	0.020	0.0014	2.207	0.015	3591 (859)	−180 (−43)	
IniII	0.183	0.098	0.435	0.0014	2.207	0.016	33596 (8036)	456 (109)	
IniIII	0.357	0.273	0.687	0.0014	2.209	0.020	127875 (30592)	619 (148)	
IniIV	0.343	0.261	0.665	0.0014	2.208	0.017	118215 (28281)	719 (172)	
Restrained dynamics									
⟨RDI⟩	0.012 ± 0.002	0.012 ± 0.001	0.004 ± 0.002	0.0015 ± 0.0001	4.15 ± 0.24	0.60 ± 0.05	138 ± 25 (33 ± 6)	209 ± 88 (50 ± 21)	
⟨RDII⟩	0.011 ± 0.001	0.012 ± 0.001	0.008 ± 0.003	0.0016 ± 0.0002	5.95 ± 0.27	0.54 ± 0.06	125 ± 17 (30 ± 4)	217 ± 58 (52 ± 14)	
⟨RDIII⟩	0.020 ± 0.002	0.019 ± 0.02	0.024 ± 0.07	0.0022 ± 0.0004	7.10 ± 1.02	0.82 ± 0.10	401 ± 67 (96 ± 16)	581 ± 251 (139 ± 60)	
⟨RDIV⟩	0.020 ± 0.001	0.018 ± 0.001	0.027 ± 0.001	0.0027 ± 0.0001	9.20 ± 0.20	0.94 ± 0.05	380 ± 42 (91 ± 10)	644 ± 88 (154 ± 21)	

membrane, the first formed by residues T5, F6, T7 and L10, and the second by residues L19, L22, L23 and L26. Between these two hydrophobic regions is a surface of charged and polar residues which could serve to make appropriate hydrogen bonding and electrostatic interactions with the membrane-bound protein receptor.

Concluding remarks

In this paper we have shown that short range ($|i-j| \leq 5$) interproton distance restraints involving only NH, $C^{\alpha}H$ and $C^{\beta}H$ protons are capable of defining, with certain limits, the overall conformation of an extended non-globular peptide. In addition, we could demonstrate that restrained molecular dynamics is an effective method for carrying out such a structure determination based on only short-range restraints. The power of this approach is due to two factors: (a) it has a large convergence radius thereby enabling the NOE restraints to effectively guide the folding to final structures which are located in the global minimum region; (b) the empirical energy function ensures approximately correct stereochemistry and non-bonded interactions once the global minimum region has been located. The largest variability occurs at the junctions of different secondary structure elements and arises from the fact that only small changes in the ϕ, ψ angles of the junction residues are required to induce relatively large positional changes of one element relative to another.

We thank Dr W. Koenig (Hoechst AG) for the gift of secretin and the Max-Planck-Institut für Plasma-Physik (Garching) for CRAY-XMP computing facilities. This work was supported by the Max-Planck-Gesellschaft, grant 321/4003/0318909A from the *Bundesministerium für Forschung und Technologie* and grant Cl 86/1-1 from the *Deutsche Forschungsgemeinschaft* (GMC and AMG).

REFERENCES

1. Kaiser, E. T. & Kezdy, F. J. (1984) *Science (Wash. DC) 223*, 249–257.
2. Robinson, R. M., Blakeney, E. W. & Mattice, W. L. (1982) *Biopolymers 21*, 1217–1228.
3. Braun, W., Wider, G., Lee, K. H. & Wuthrich, K. (1983) *J. Mol. Biol. 169*, 921–948.
4. Clore, G. M., Martin, S. R. & Gronenborn, A. M. (1986) *J. Mol. Biol. 191*, 553–561.
5. Gronenborn, A. M., Bovermann, G. & Clore, G. M. (1987) *FEBS Lett. 215*, 88–94.
6. Havel, T. F. & Wuthrich, K. (1985) *J. Mol. Biol. 182*, 281–294.
7. Braun, W. & Go, N. (1985) *J. Mol. Biol. 186*, 611–626.
8. Clore, G. M., Brunger, A. T., Karplus, M. & Gronenborn, A. M. (1986) *J. Mol. Biol. 191*, 523–551.
9. Clore, G. M., Gronenborn, A. M., Brunger, A. T. & Karplus, M. (1985) *J. Mol. Biol. 186*, 435–455.
10. Kaptein, R., Zuiderweg, E. R. P., Scheek, R. M., Boelens, R. & van Gunsteren, W. F. (1985) *J. Mol. Biol. 182*, 179–182.
11. Clore, G. M., Nilges, M., Sukumaran, D. K., Brunger, A. T., Karplus M. & Gronenborn, A. M. (1986) *EMBO J. 5*, 2729–2735.
12. Clore, G. M., Sukumaran, D. K., Nilges, M., Zarbock, J. & Gronenborn, A. M. (1987) *EMBO J. 6*, 529–537.
13. Jeener, J., Meier, B. H., Bachmann, P. & Ernst, R. R. (1979) *J. Chem. Phys. 71*, 4546–4553.
14. Marion, D. & Wuthrich, K. (1983) *Biochem. Biophys. Res. Commun. 113*, 967–974.
15. Brooks, B. R., Bruccoleri, R. E., Olafson, B. D., States, D. J., Swaminathan, S. & Karplus, M. (1983) *J. Comput. Chem. 4*, 187–217.
16. Williamson, M. P., Havel, T. F. & Wuthrich, K. (1985) *J. Mol. Biol. 182*, 295–315.